QUARTERLY JOURNAL OF THE ROYAL METEOROLOGICAL SOCIETY
Q. J. R. Meteorol. Soc. **133**: 1615–1627 (2007)
Published online 5 September 2007 in Wiley InterScience
(www.interscience.wiley.com) DOI: 10.1002/qj.138

RMetS
ROYAL METEOROLOGICAL SOCIETY

Role of nocturnal turbulence and advection in the formation of shallow cumulus over land

Jordi Vilà-Guerau de Arellano*
Wageningen University, The Netherlands

ABSTRACT: Shallow cumuli over land are normally studied from a diurnal perspective. However, the thermodynamic vertical profiles of the morning transition may play an important role in setting up favourable conditions for the formation of shallow cumuli. In turn, these profiles are highly dependent on the evolution of the nocturnal boundary characteristics and of their layer aloft.

By analysing thermodynamic profiles measured by radiosondes launched every three hours at four different stations, we are able to determine how horizontal advection and turbulent mixing modify the atmospheric stability and the differences in potential temperature and specific humidity at the interface between the atmospheric boundary layer and the layer above it. Two consecutive nights are studied. They show very similar boundary-layer development; but variations in the layer aloft by a low-level-jet advection event during the second night, and intense turbulent mechanical mixing, lead to the development of two diurnal boundary layers with very different characteristics: the first one clear, the second cloudy.

To complete the observational study, we perform a sensitivity analysis using a mixed-layer model to examine the role of the morning initial conditions in the formation of shallow cumuli over land. The complexity and subtlety of the observed situation – namely, the interaction of a strongly-mixed nocturnal boundary layer and horizontal advection – make this case suitable for testing the capacity of mesoscale models to reproduce cloudy boundary layers that are largely dependent on conditions during the previous night. Copyright © 2007 Royal Meteorological Society

KEY WORDS shallow cumulus; mesoscale boundary-layer interaction; nocturnal boundary layer; morning transition

Received 2 March 2007; Revised 3 July 2007; Accepted 6 July 2007

1. Introduction

The formation and further development of shallow cumuli over land are driven by the daily variations in surface turbulent fluxes. Their evolution is also dependent on the thermodynamic characteristics, and on the atmospheric stability within and above the atmospheric boundary layer. To date, studies have focused on the role of the land–atmosphere interaction in controlling shallow-cumulus formation (Ek and Holtslag, 2004), and on the main dynamic characteristics and controlling processes (Zhu and Albrecht, 2002, 2003; Brown *et al*., 2002). Compared with the formation of fair-weather cumuli above maritime conditions, shallow cumuli above land are highly dependent on the diurnal cycle of the boundary layer, external forcings, and the horizontal variability of surface properties. Therefore – and because of their non-steady development – their representation in large-scale models is more problematic than for those above the sea (Neggers *et al*., 2004; Lenderink *et al*., 2004; Berg and Stull, 2006).

However, one important set of conditions – the initial morning characteristics of the thermodynamic vertical structure – has received little attention, particularly with regard to how the structure of the nocturnal boundary layer (NBL) and the layer above it evolve to establish the optimal stability conditions for triggering shallow-cumulus formation during the day. As mentioned by Zhu and Albrecht (2002), weaker stratification and an inversion potential-temperature jump contribute to a small positive-feedback processes in cloud formation. Both are largely dependent on the initial thermodynamic state at dawn. In this paper, we present observational evidence of these feedback mechanisms during the transition from nocturnal to diurnal boundary-layer conditions.

In order to assess the influence of the NBL on shallow cumulus over land, two consecutive nights have been studied, using detailed surface and upper-air observations. The measurements were taken at the Southern Great Plains Atmospheric Radiation Measurement (ARM) site in Oklahoma and Kansas, USA. The high spatial distribution (four radiosonde launching stations within 200 km of the central facility) and high temporal frequency (with a radiosonde being launched every 3 h) make the ARM site particularly suitable for our purposes. Moreover, the ARM site has been used before to study cloudy boundary layers over land (Zhu and Albrecht, 2002).

The nights studied are those of 19–20 and 20–21 June 1997. Although they present very similar characteristics in synoptic and mesoscale terms, differences above the

* Correspondence to: Jordi Vilà-Guerau de Arellano, Meteorology and Air Quality Section, PO Box 47, 6700 AA Wageningen, The Netherlands. E-mail: jordi.vila@wur.nl

Copyright © 2007 Royal Meteorological Society

WILEY InterScience® DISCOVER SOMETHING GREAT

NBL, and intense turbulent mixing in the NBL, lead to the development of two diurnal boundary layers with very different turbulent characteristics. On the first night, a cloudless boundary layer is formed, with a high rate of entrainment, driven partly by shear at the surface and at the inversion zone (Pino *et al*., 2003). On the second night, shallow cumuli are observed, with a coverage of 20%–30% above the ARM site (Zhu and Albrecht, 2002; Brown *et al*., 2002).

The primary goals of this study are:

- to analyse the observational evidence of the role of advection and turbulent mixing during the night in establishing the conditions required for the formation of daily shallow cumuli; and
- to examine, through a sensitivity analysis, the dependence of cloud development on the initial morning atmospheric stability and properties within the entrainment region.

2. The large-scale meteorological situation during the two nights

In terms of the boundary layer, the two nights studied present similar characteristics, as we will discuss in more detail in the next section. It is therefore necessary first to analyse their synoptic and mesoscale conditions. As Nakamura and Mahrt (2006) have recently pointed out, mesoscale phenomena can have a large effect on the dynamics and structure of the NBL. The synoptic and mesoscale situation for the nights of 19–20 June and 20–21 June at 06 LT (throughout this paper, LT (local time) stands for UTC minus 6 h.) is shown in Figures 1 (sea-level pressure and horizontal wind vectors at 1000 m) and 2 (potential temperature and water-vapour mixing ratio at 1000 m). The three days are modelled by means of the mesoscale model MM5 version 3.6 (Dudhia, 1993). ECMWF data are used to initialize and update the boundary conditions every 6 h. Boundary-layer turbulent fluxes are represented using the Medium-Range Forecast scheme coupled to a simple land-use model. The other important physical parametrizations are the Kain–Fritsch scheme for convection and a simple ice scheme for the microphysical processes. Both figures show the biggest domain (an approximately-square region of 1674×1674 km^2) discretized with a grid length of 54 km. A 24 h spin-up is applied to allow the physical parametrization to adapt to initial and boundary conditions. The central facility of the ARM site is located at the centre of the domain (grid point (15, 15), indicated by the letter C in Figures 2 and 4).

Figure 1 shows that the two nights are characterized by low pressure to the northwest of the area under study. By the second night, the centre of the low has moved steadily southward (approximately 50 km). The horizontal wind vectors at 1000 m show similar wind direction (190°) and strength (15–20 ms^{-1}) at the centre of the domain (grid point (15, 15)). These strong winds are associated

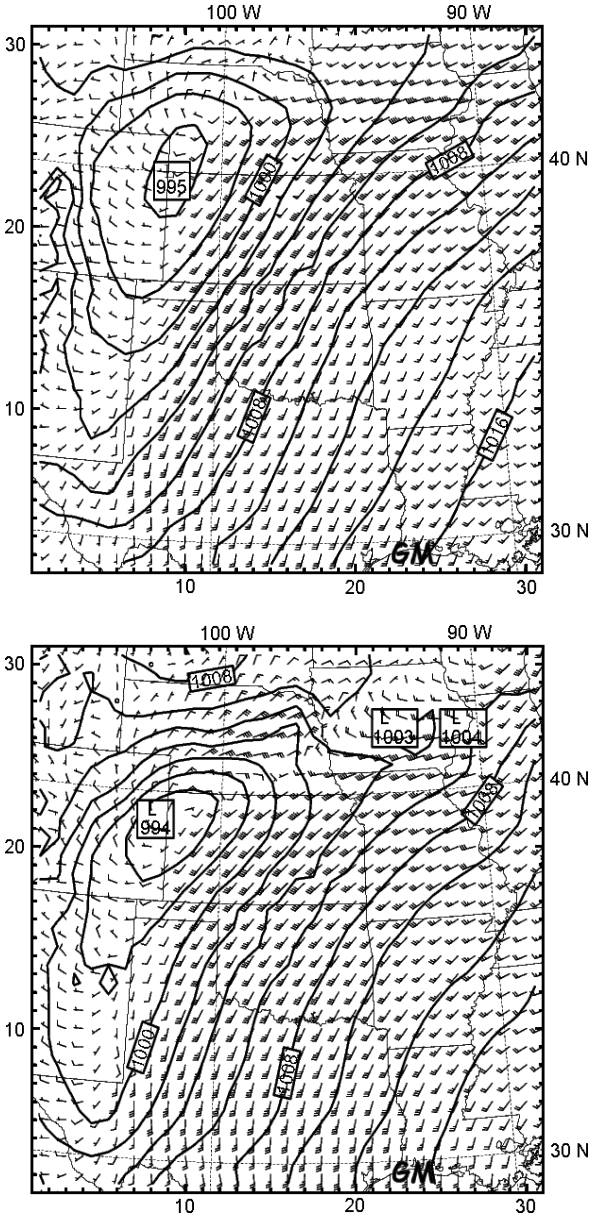

Figure 1. Maps of sea-level pressure (mb) and horizontal wind vectors at 1 km, calculated using the mesoscale model MM5, for 06 LT on 20 June (upper panel) and 21 June (lower panel). Each full barb of the wind vector represents 5 ms^{-1}. GM indicates the Gulf of Mexico.

with the presence of an observed low-level jet (LLJ) (see Section 3.2, Figure 8, for further discussion).

Figure 2 shows the potential-temperature field and the mixing ratio of water vapour at 1000 m above ground level. We have chosen this height as it is representative of changes in potential temperature and moisture above the NBL. Although the spatial pattern of potential temperature is similar, the model results show that at the centre of the domain the air has become colder by approximately 2 K: on 20 June at the central site C, the potential temperature is above 307 K, whereas on 21 June it has fallen to 305 K. The water-vapour content also increases: from 13 g/kg on 20 June to 14 g/kg on 21 June. The absence of precipitation at C on 20 June eliminates the possibility of an increase in soil

Copyright © 2007 Royal Meteorological Society

DOI: 10.1002/qj

moisture availability, and therefore of the latent heat flux at the surface. Another factor that could cause these changes in the potential temperature and water-vapour content is the heterogeneity of the surface conditions. It is known that the central site C is characterized by a strong west–east variation in the Bowen ratio (Cheinet *et al*., 2005). However, in our meteorological situation both nights are dominated by the same south-southwest component, so this effect is minimal.

The relative proximity of the Gulf of Mexico (approximately 450 km southeast of C, marked GM in Figure 1) may be the cause of the colder and wetter air masses. In Figure 1, a slight veering can be observed in the wind direction between 20 and 21 June, from 190° to 170°. According to the mesoscale modelling results, this entering of cold and wet air above the boundary layer at C starts at around 02 LT. This turning of the wind towards the east could be the origin of the advection of maritime air towards C. In this respect, we have a particular case of a phenomenon documented by Higgins *et al*. (1997) and Cheinet *et al*. (2005).

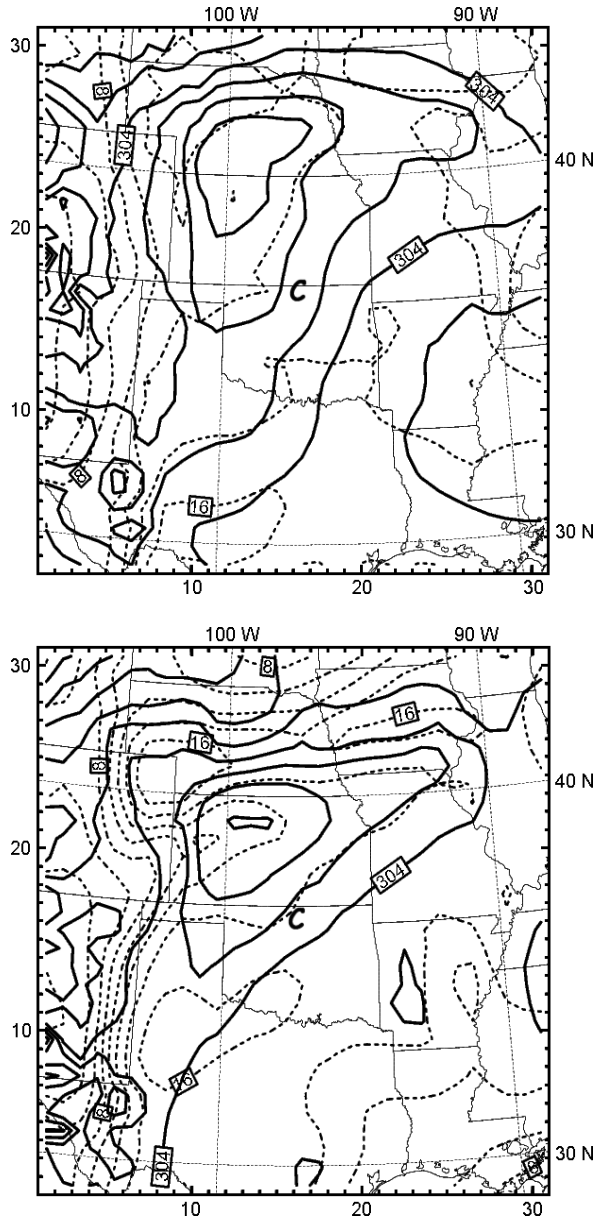

Figure 2. Maps of potential temperature (K, continuous lines) and water-vapour mixing ratio (g/kg, dashed lines) at 1 km, calculated using the mesoscale model MM5, for 06 LT on 20 June (upper panel) and 21 June (lower panel). The contour interval for potential temperature is 2 K, and that for water-vapour mixing ratio is 2 g/kg. C indicates the location of the central facility of the ARM site.

To complete this discussion, Figure 3 shows the horizontal advective tendencies calculated using the ECMWF model (ERA-40 reanalysis) at C (Uppala *et al*., 2005). The period of the large-scale forcing is 6 h. Since we are focusing on the differences in behaviour between the two nights, we select the following times: 00 LT (06 UTC) and 06 LT (12 UTC). In agreement with the MM5 results, the large-scale horizontal heat advection (Figure 3(a)) shows a more significant drying tendency for the first night. In the analysed period, the region above the LLJ (at 500–1000 m) is warmed, with a heating rate of 0.2–0.55 Kh^{-1}. As we discuss in the next section, this large-scale forcing favours the creation of a stronger inversion during the morning transition, preventing cloud formation. The following night shows a transition between cooling and heating below 1000 m, but above 1000 m it maintains a cooling tendency, which increases the atmospheric instability above this height.

The drying that takes place on the night of 19–20 June is also more significant than that of the following night (Figure 3(b)), particularly at heights of 1000–2000 m, which could favour the cloudless conditions observed on 20 June. During the night of 20–21 June, the increase of moisture in the boundary layer (shown also in Figure 2) is an additional positive tendency in establishing appropriate conditions for cloud formation during 21 June. In the next section, we will analyse, and discuss in more detail, the specific surface forcing measured at C and the temporal and (vertical) spatial distribution of the thermodynamic variables.

3. Vertical profiles of thermodynamic variables: temporal evolution and spatial distribution

This study relies heavily on the dense spatial distribution and high temporal frequency of the radio-soundings (a sonde was launched every 3 h). Figure 4 shows the locations of the four sites selected for this study, as well as the topography, which is characterized by a gentle east–west slope. The maximum distance between the central facility C and the the other stations is approximately 200 km. In addition to the upper-air measurements, surface-mean and turbulent-flux variables were measured continuously at C.

3.1. Surface forcing and boundary-layer characteristics

The two nights studied are characterized by similar surface forcing and atmospheric stability in the NBL. Figure 5 shows the temporal evolution of the sensible

Copyright © 2007 Royal Meteorological Society

DOI: 10.1002/qj

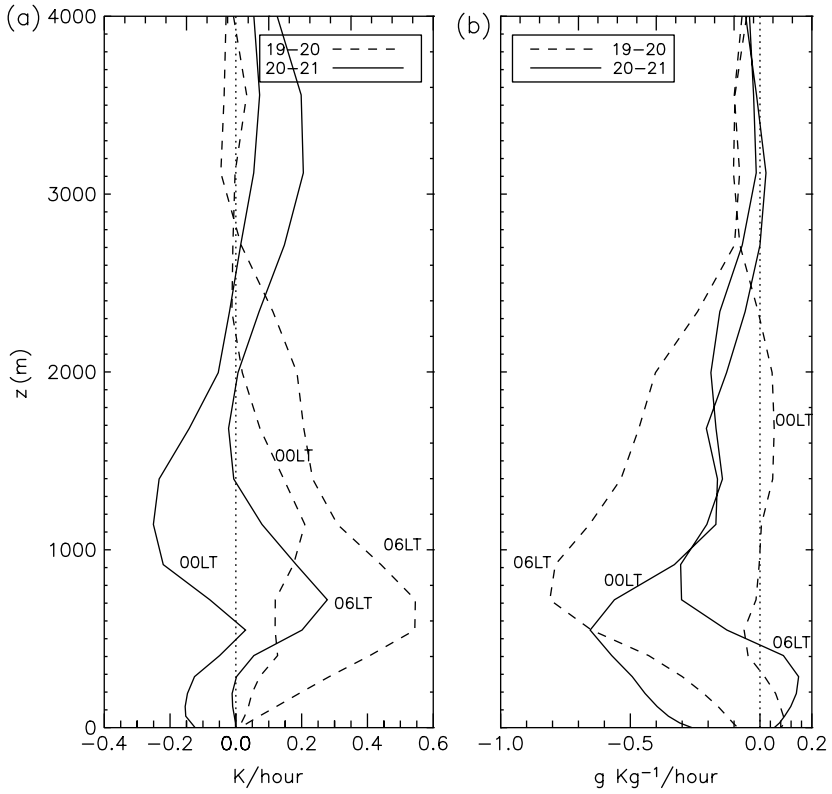

Figure 3. Horizontal advection of (a) heat and (b) specific moisture, as derived from the reanalysis of the ECMWF model at the central facility C of the ARM site.

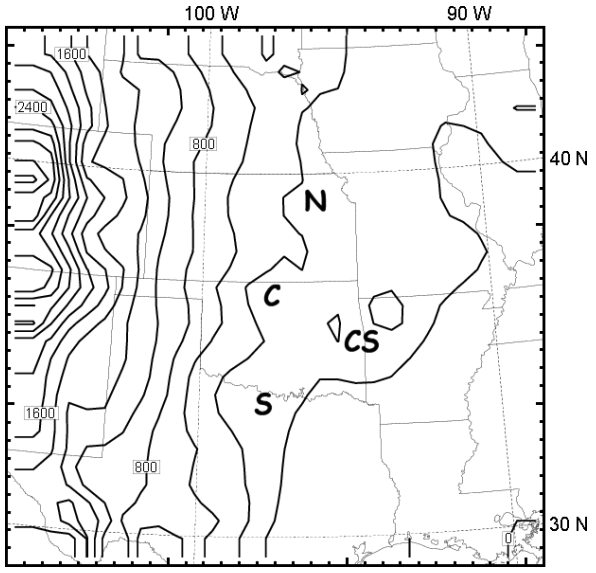

Figure 4. Topography, and locations of the radiosonde station facilities: C (36.605 °N, −97.485 °W, 315 m), S (34.969 °N, −97.415 °W, 344 m) N (38.305 °N, −97.301 °W, 447 m), CS (35.688 °N, −95.856 °W, 217 m).

heat flux, the temperature measured at 2 m, and the friction velocity. The half-hour turbulent surface fluxes are measured using a fast-response three-dimensional sonic anemometer, and the water-vapour density is measured using an open-path infrared gas analyser. The sensible heat flux is almost constant over time, with values in the range $-40--50$ Wm^{-2}. The latent heat flux shows a similar constant behaviour over time on both nights, with a value of 30 Wm^{-2} (not shown). Clouds are not observed on either night, and the surface long-wave radiative cooling shows very similar temporal evolution on the two nights, with a linear rate of fall in temperature of about 0.4 Kh^{-1}. High friction velocities are measured, these being driven by high shear on both nights (see Figure 8). Values are almost constant over time (around 0.6 ms^{-1}), and the main difference is in the minimum value of the friction velocity u_* at around 03:30 LT on 21 June, though it has a tendency to increase towards values similar to those of the previous night. The vertical profiles of the mean wind measured by the radiosondes corroborate these large night-time values (see Section 3.2, Figure 8).

Table I summarizes the surface turbulent fluxes, scaling parameters and other relevant boundary-layer characteristics. We have defined the boundary-layer depth on the basis of the location of the LLJ, the wind-speed maximum (see Figure 8). As indicated by the scaling parameters h/L and the gradient of the Richardson number, both NBLs are dominated by strong turbulent mixing driven by wind shear, and can thus be classified as weakly stable.

3.2. Temporal evolution

Figure 6 shows the temporal sequence (23 LT, 02 LT, 05 LT, 08 LT) of the vertical profiles of potential temperature at C during the two consecutive nights. In order to distinguish between the evolution of the profiles within

Copyright © 2007 Royal Meteorological Society

DOI: 10.1002/qj

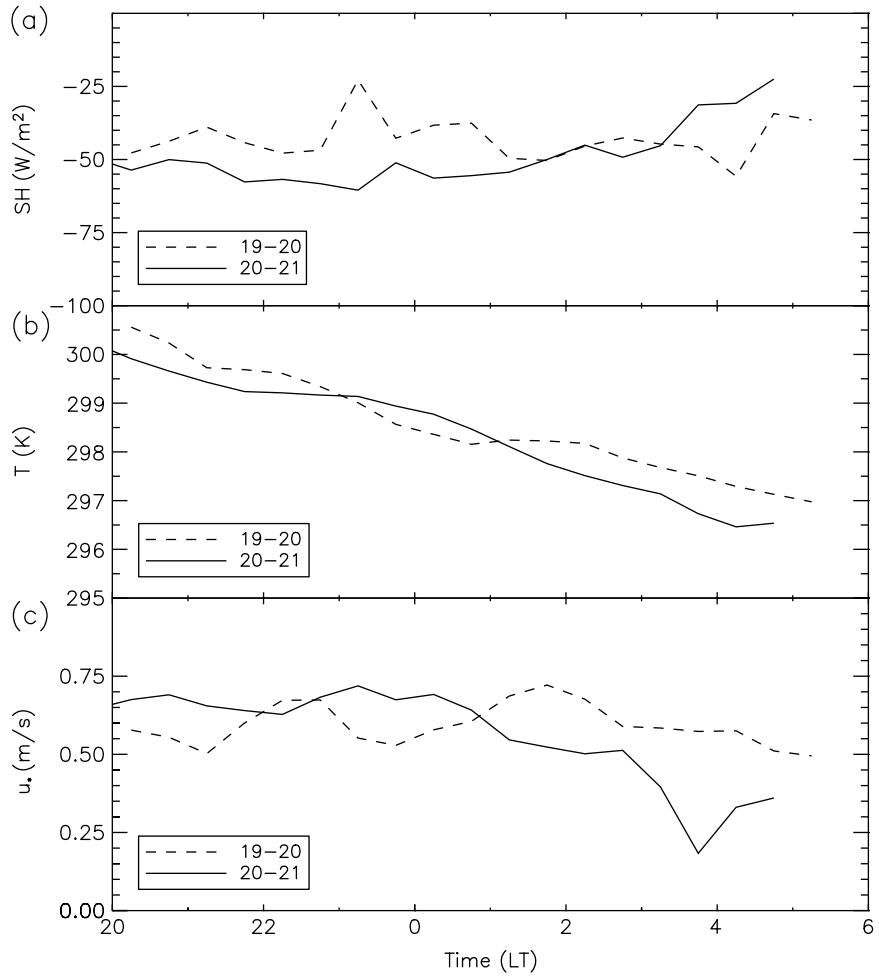

Figure 5. Temporal evolution during the two consecutive nights, at the central site C, of: (a) sensible heat flux; (b) temperature at 2 m; (c) friction velocity.

Table I. Turbulent surface fluxes (sensible $w'\theta'_o$; latent $w'q'_o$ and friction velocity u_*) and boundary-layer scaling variables (boundary layer height h; gradient Richardson number Ri_g, Monin-Obukhov length L and low-level jet LLJ). Values are averaged over the whole night, except for the boundary-layer height h, the gradient Richardson number Ri_g, Monin-Obukhov length L, and the low level jet LLJ value estimated from the two radio-soundings at 02 LT.

Night (June)	h (m)	$\overline{w'\theta'}_o$ (Wm^{-2})	$\overline{w'q'}_o$ (Wm^{-2})	u_* (ms^{-1})	LLJ (ms^{-1})	h/L	Ri_g
19–20	500	−41.9	30	0.59	24.0	1.06	0.16
20–21	450	−48.5	29	0.55	23.0	1.37	0.15

and above the NBL, the figure also shows the boundary-layer height h, estimated as the height of the mean wind maximum (LLJ). The similar evolution of the long-wave radiative cooling and intense vertical mixing within the NBL yields very similar developments of the stable stratification in the NBL during the two nights. Above the NBL, the θ profile at 23 LT during the first night is slightly colder. However, at 02 LT, the two profiles are almost identical, having the same boundary-layer height, and slightly higher stability values for the second night.

On 21 June, between 02 LT and 05 LT the air mass above the NBL cooled significantly. For instance, if we take 1000 m as a reference height, we observe that during the night of 19–20 June, θ remains almost constant (about 312 K), whereas during the second night it has decreased by 4 K. Closely associated with this cooling is an increase in the instability of the upper layer.

The temporal evolution of the specific-moisture profiles is similar (Figure 7). The drier layer above the NBL during the night of 20–21 June differs from that of the first night by a large increase in moisture content: from 5 g/kg to 15 g/kg at 1000 m during the period 02–05 LT. At 05 LT on 21 June, except for the maximum and minimum values of the specific humidity at 650 m and 1000 m respectively, we observe higher water-vapour content up to a height of 1300 m, well above the NBL. Furthermore, the strong mechanical turbulent mixing within the NBL leads to a well-mixed layer on both nights: the difference between the values at the surface and at the top of the NBL is less than 1 g/kg, because the (positive) moisture flux is almost constant over time.

To complete our analysis of Figure 6, the vertical specific-moisture profile at 08 LT on 21 June once again demonstrates the establishment of optimal conditions for the formation of shallow cumulus: a well-mixed profile

Copyright © 2007 Royal Meteorological Society

DOI: 10.1002/qj

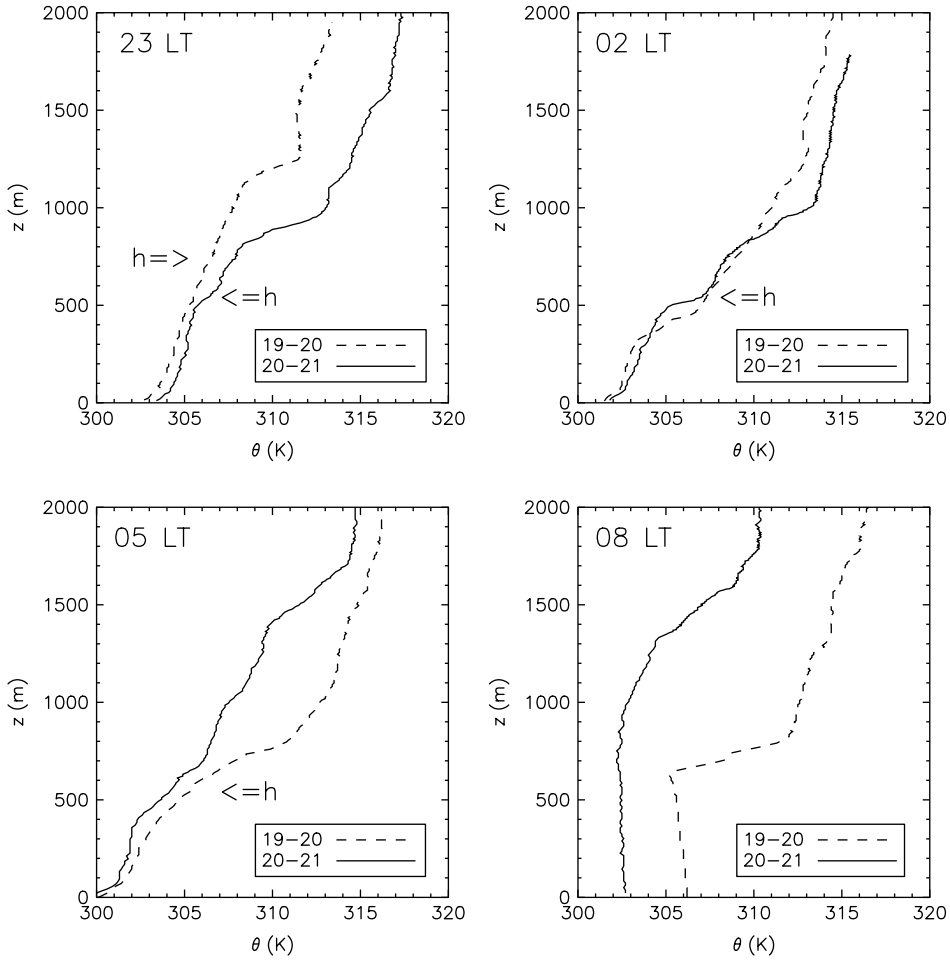

Figure 6. Temporal evolution of the vertical potential-temperature profiles at C during the nights of 19–20 and 20–21 June. The boundary-layer height h is also indicated. At 02 LT and 05 LT, the boundary-layer height is the same (500 m) on both nights.

up to 1500 m, with high water-vapour content (about 15 g/kg).

Finally, Figure 8 shows the temporal evolution of the vertical profiles of wind speed on the two nights. A common pattern is shown by the larger shear values below and above the LLJ for both nights, yielding well-mixed vertical profiles of specific humidity. As discussed by Conangla and Cuxart (2006), the LLJ generates mechanical turbulence, which induces weakly-stable stratification below and above the NBL. At 23 LT, one can observe the initial formation of the LLJ at a height of 500 m. At 02 LT, as with the potential-temperature and specific-humidity profiles, the variation of the height of the wind is very similar during the two nights. The LLJ has a value of 24 ms^{-1} located at the same height, around 500 m. At 05 LT, the LLJ has almost disappeared during the first night, and it has decreased to 20 ms^{-1} during the second night. Well-mixed wind profiles are observed 2 h after sunrise (08 LT), with surprisingly lower values for 21 June. We have investigated the possible reasons for these low values. The vertical profile at 11 LT (not shown) is once again characterized by values similar to those of 20 June, with an averaged vertical value of 10 ms^{-1}. For 08 LT, Figure 8 also shows the vertical profiles calculated from the mesoscale model MM5. The agreement with the observations of 20 June is very satisfactory. Moreover, we find very similar values for the modelled mean wind profiles during the two days. We conclude that the observed values of the second day are probably affected by an instrumental error, and should be disregarded.

Finally, the wind direction (not shown) hardly varies with height or time, maintaining an almost constant value of 200°, in close agreement with the horizontal wind vectors shown in Figure 1.

3.3. Spatial distribution

The altitude differences of θ and q for the four radiosondes launched at stations S, CS, C and N on 21 June at 02 LT and 05 LT are shown in Figures 9 and 10 respectively. At the four sites, the NBL height is around 500 m at 02 LT. In the NBL, C and S are 1 K colder, but the stable stratification has similar values. Above the NBL, C and N show warmer and more stable stratified profiles. The specific-humidity observations (Figure 9(b)) confirm these differences between C and N and between S and CS. Slightly above the temperature inversion jump at 500 m, much drier air is found at C and N, with a sharp decrease to 6 g/kg at around 800 m. Within the NBL,

Copyright © 2007 Royal Meteorological Society

DOI: 10.1002/qj

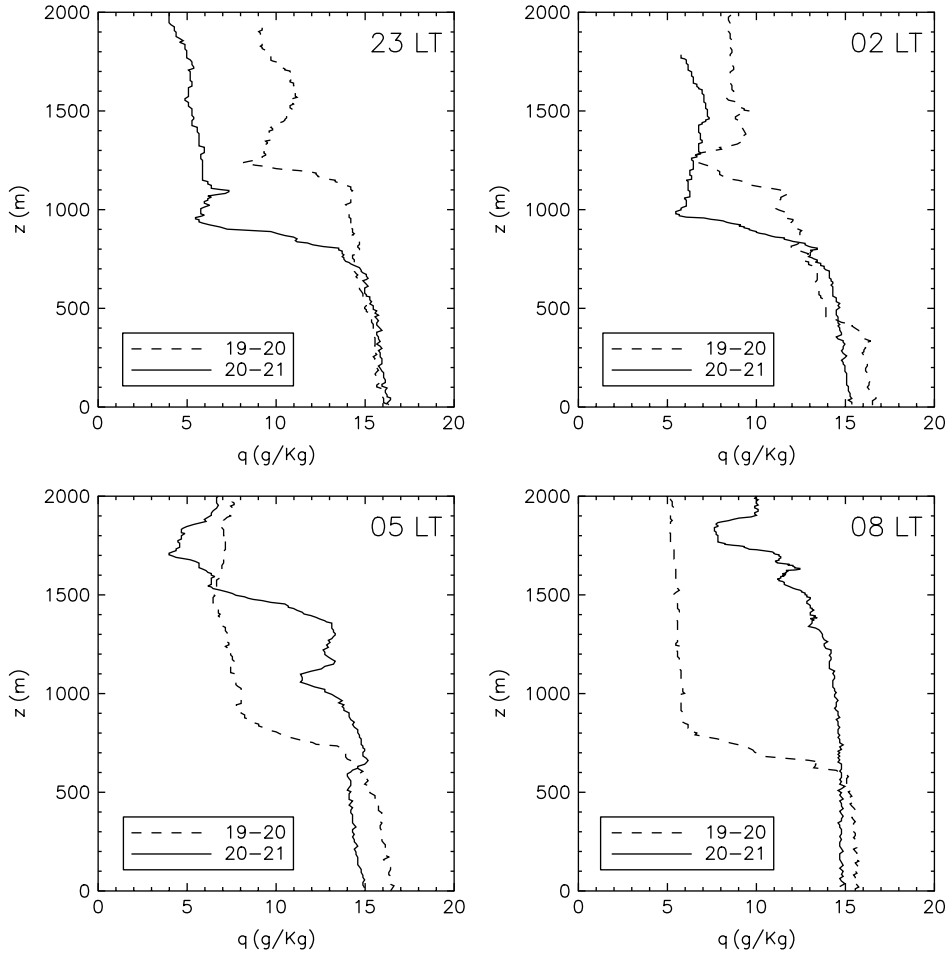

Figure 7. As Figure 6, but showing specific humidity.

the four q profiles indicate a well-mixed layer, with an average value of around 15 g/kg, except at N, which shows higher values.

Three hours later, at 05 LT, the θ profiles are almost identical at the four sites in the whole region under study. At sites S and CS and above 500 m, the vertical variation in potential temperature has hardly changed, whereas colder air – a decrease of almost 6 K at 1000 m – is measured above C and N. Within the NBL, very similar slopes are found for the variation of potential temperature with height. At 05 LT, the lifting condensation level (LCL) at C is located at 500 m, near the top of the NBL.

Figure 10(b) also shows a large difference in the moisture content above C and N, with an increase of almost 10 g/kg during the period 02–05 LT. Except for the sonde launched at N, the measured profiles are relatively well mixed up to 1000 m. Above this altitude, the moisture content decreases, reaching a value of 5 g/kg at 1500 m.

Knowledge of the spatial distributions of the potential-temperature and specific-humidity profiles within a radius of 200 km from the central site C allows us to monitor the modification of the layer above the NBL at C. Between 02 LT and 05 LT, colder and moister air is advected by the LLJ over this site. As Figure 1 shows, the characteristics of this air mass are probably maritime, originating in the Gulf of Mexico. This modification of the upper layer tends to favour the formation of shallow cumulus in diurnal conditions. Compared with the previous night, the modifications in the layer above the NBL have decreased the height of the LCL (by 200 m – see Figure 11) by cooling it down and enhancing its moisture content.

Moreover, the layer above the NBL becomes more unstable, and the jump in potential temperature and specific humidity at the inversion is reduced. The intense turbulent mixing in the NBL is an additional factor that maintains relatively well-mixed profiles of potential temperature and specific humidity throughout the night. In consequence, the smaller gradients of virtual potential temperature favour the rapid formation of a convective boundary layer during the morning transition. This observed situation emphasizes the subtlety of the formation of shallow cumuli in the boundary layer, in which modifications occurring during the previous night can produce conditions favourable for the formation of boundary-layer clouds.

3.4. Early-morning profiles

It is convenient to end our discussion by showing the vertical profiles of potential temperature at 08 LT (2 h after

Copyright © 2007 Royal Meteorological Society

DOI: 10.1002/qj

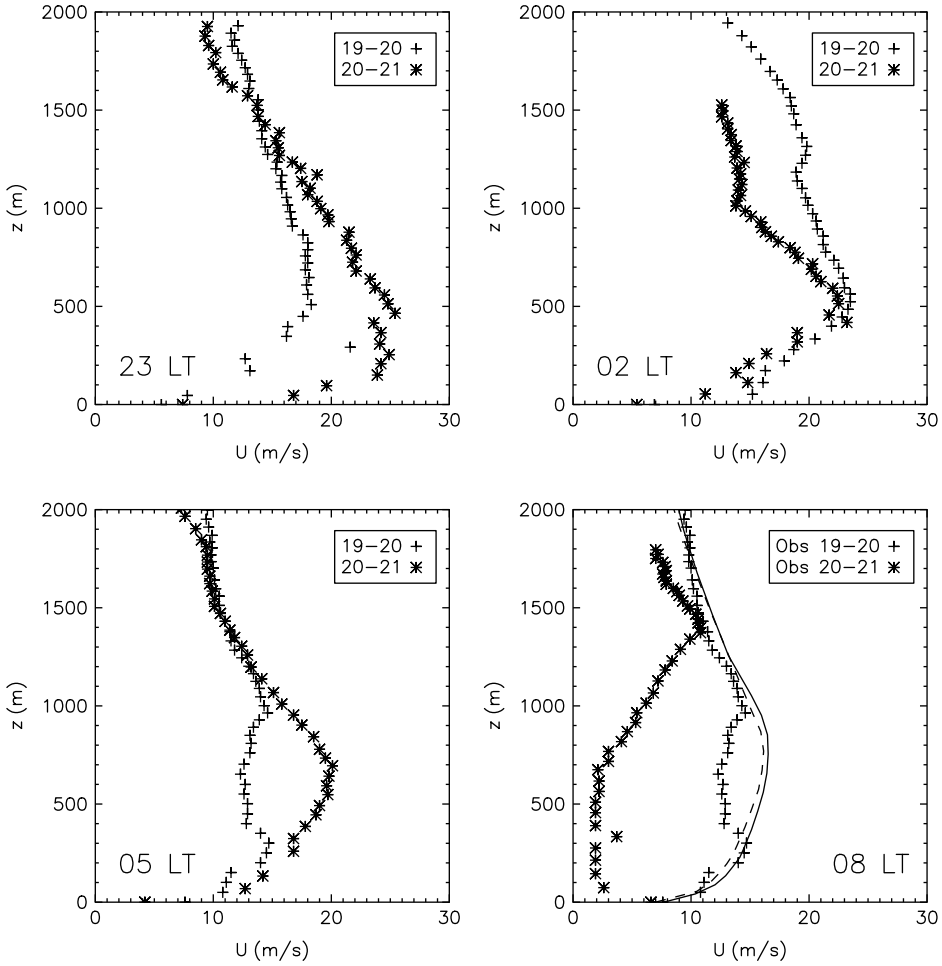

Figure 8. As Figure 6, but showing wind speed. The panel for 08 LT also shows the results given by the MM5 model, for 20 June (continuous line) and 21 June (dashed line).

sunrise) in relation to atmospheric stability (Figure 11). Several large-eddy simulation studies (Brown *et al*., 2002; Pino *et al*., 2003), and the single-column model intercomparison study (Lenderink *et al*., 2004), have used these θ profiles as initial profiles for the purposes of studying the structure and evolution of diurnal boundary layers. Thus, these profiles are already determining the main characteristics of the diurnal development of the boundary layer. Up to 650 m (20 June) and 1000 m (21 June), both profiles show a well-mixed layer driven by convection (convective velocity scale w_* values of 1.16 ms^{-1} and 1.38 ms^{-1} respectively) and by mechanical turbulence due to the high winds (u_* values of 0.6 ms^{-1} and 0.5 ms^{-1} respectively). Above these heights, the potential-temperature profiles show distinct features. A strong capping inversion ($\Delta\theta = 6$ K) limits the growth of the convective boundary layer in the early morning hours of 20 June. The specific characteristics of the sounding already determine the future development of a clear boundary layer, which inhibits a rapid growth of the boundary layer in the early morning hours (approximately 100 m/h). However, as Pino *et al*. (2003) have stressed, this boundary-layer growth rate is later increased to values close to 166 m/h because of the contribution of shear to the entrainment of heat: see the vertical profiles of mean wind in (Pino *et al*., 2003, figure 5); this figure also shows the moist adiabatic lapse rate, indicating an LCL at 1200 m, 500 m above the top of the convective boundary layer. Therefore, the strong inversion potential-temperature jump, and the warm and dry characteristics above the boundary layer, resulting from the night-time thermodynamic evolution, lead to a cloudless diurnal boundary layer.

The profile for 21 June already presents optimal conditions for the formation of shallow cumulus: an LCL (at 900 m) below the inversion ($h = 1000$ m); absence of a potential-temperature jump at the top of the mixed layer; a slope exceeding the moist adiabatic lapse rate (i.e. conditionally unstable); and the possibility of vertical development of the potential cloud up to a height of 1600 m (the limit of convection). In their study of shallow cumulus over land, Brown *et al*. (2002) take into account some of these vertical characteristics in defining the initial profile of the potential temperature. Except in a small layer between 1400 m and 1500 m, their θ profile has a slope similar to that of the observed sounding of 21 June, and it also lacks a clear potential-temperature jump at the interface between the boundary layer and the free troposphere.

Copyright © 2007 Royal Meteorological Society

DOI: 10.1002/qj

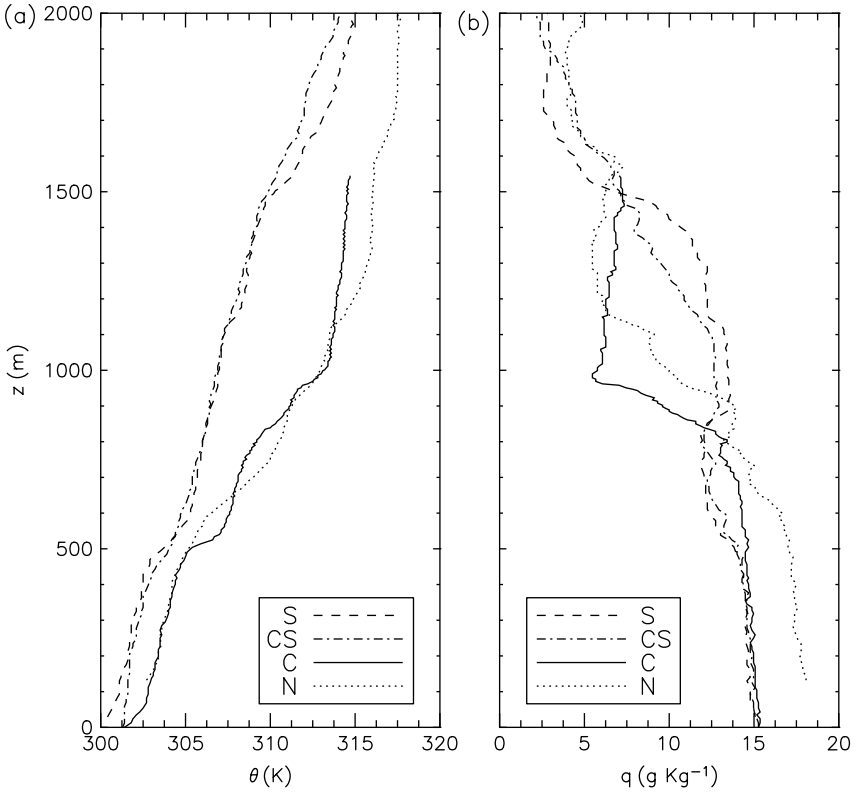

Figure 9. Vertical profiles of (a) potential temperature and (b) specific humidity, at the sites S, CS, C and N, at 02 LT on 21 June.

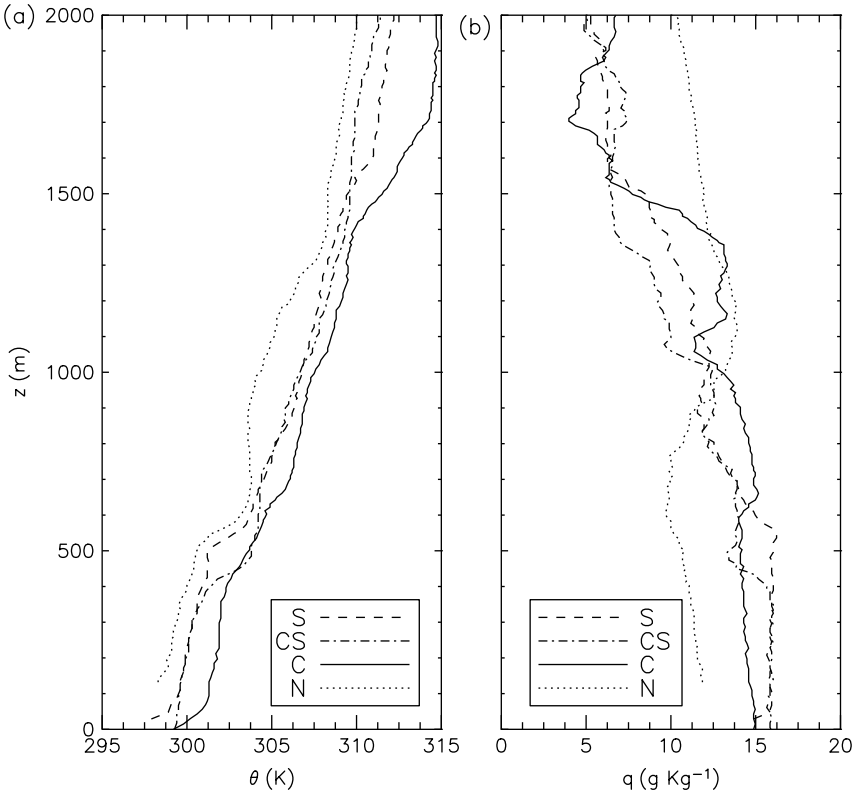

Figure 10. As Figure 9, but at 05 LT.

Copyright © 2007 Royal Meteorological Society

DOI: 10.1002/qj

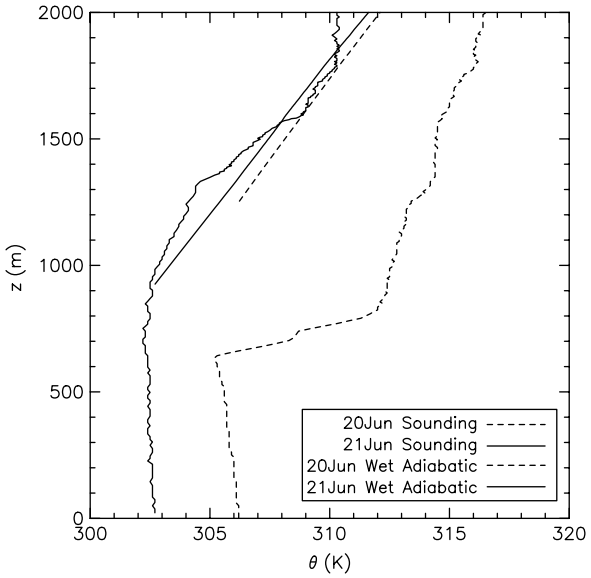

Figure 11. Vertical profiles of potential temperature 2 h after sunrise (08 LT). The moist adiabatic profiles are also shown.

4. Dependance of cloud formation on initial morning conditions

As shown by the analysis above, thermodynamic modifications of the layer above the NBL result in wide variations in the vertical distribution of potential temperature and moisture content. The morning transition conditions are influenced by these variations: particularly by the formation of the initial interface jumps in potential temperature ($\Delta\theta_{vo}$) and moisture (Δq_o) during the early stages of development of the convective boundary layer. These nocturnal variations have a strong influence on the further evolution of the boundary-layer growth, and are thus responsible for setting up the optimal conditions for the formation of boundary-layer clouds once diurnal convection has begun. Here, we carry out a sensitivity analysis to study the dependence of boundary-layer height and LCL on the initial values of the potential-temperature and moisture jumps at the interface and the potential-temperature lapse rate.

A mixed-layer model (Lilly, 1968; Tennekes, 1973) is used to calculate the boundary-layer evolution and to estimate whether water vapour saturates – i.e. whether the LCL is below h (so that clouds can potentially be formed) or above h (so that clouds are absent). See Appendix A for details of the model formulation. The mixed-layer model reproduces the evolution of the slab convective-boundary-layer variables (sub-cloud layer) observed during 21 June, and it includes an explicit calculation of the time evolution of the LCL. Our approach is similar to that of Zhu and Albrecht (2002), who employ the mixed-layer model as a conceptual tool that can accurately reproduce the bulk characteristics of the convective boundary layer.

Our initial conditions for the mixed-layer model, summarized in Table II, are similar to those prescribed by Brown *et al*. (2002), so as to reproduce convective-boundary-layer conditions similar to those observed on 21 June 1997 at site C (Zhu and Albrecht, 2002; Brown *et al*., 2002).

The sensitivity tests focus on the initial values of $\Delta\theta_{vo}$, Δq_o, γ_θ, and the ratio of the entrainment heat flux to the surface heat flux, β_{θ_v}. The first three of these are strongly influenced by the arrival of the colder and moister air mass above the NBL between 02 LT and 05 LT. Figure 12 shows the time evolution of the boundary-layer height and the LCL, calculated for two different cases: $\Delta q_o = -0.5$ g/kg (close to the sunrise conditions of 21 June) and $\Delta q_o = -5.0$ g/kg (close to the sunrise conditions of 20 June). Figure 12(a) shows the model results derived from values close to the initial observations (for $\Delta q_o = -0.5$ g/kg), and the other panels show the results of the sensitivity tests. Note that in all cases the absolute decrease of the moisture jump at the inversion (from -5.0 g/kg to -0.5 g/kg) leads to a moist boundary layer (a lower LCL), because there is less entrainment of dry air into the boundary layer.

Figure 12(a) shows the evolution of h and LCL, using initial conditions close to the situation observed for 21 June (see Table II). Using an initial $\Delta q_o = -0.5$ g/kg, the model reaches the condition $h = LCL$ at around 11 LT. At approximately this time, clouds were observed over the central facility C; and the ceilometer reported a cloud-base height (similar to the LCL) of around 1000 m between 10 LT and 11 LT (see (Brown *et al*., 2002, figure 5)). A decrease in the initial jump in specific humidity ($\Delta q_o = -5.0$ g/kg) would lead to a delay of 1 h in attainment of the condition $h = LCL$, because of the entrainment of dry air and the consequent increase in the LCL.

Table II. Initial and prescribed values used for the mixed-layer model to calculate the boundary-layer height and the LCL on 21 June 1997 at site C. The parameter t_d is equal to 10 h.

Quantity	Value
h_o	700 m
w_s	0
$\langle\theta_{vo}\rangle$	301 K
$\Delta\theta_{vo}$	0.1 K
$(\overline{w\theta_v})_o$	$0.09\sin(\pi t/t_d)$ Kms^{-1}
γ_{θ_v}	3×10^{-3} K/m
β_{θ_v}	0.2
$\langle q\rangle_o$	15 g/kg
Δq_o	-0.5 g/kg
$(\overline{wq})_o$	$0.16\sin(\pi t/t_d)$ g/kg ms^{-1}
γ_q	0

h_o is the initial boundary layer height; w_s is the mean vertical subsidence velocity; $\langle\theta_{vo}\rangle$ is the initial slab virtual potential temperature; $\Delta\theta_{vo}$ is the initial virtual potential temperature jump; $(w'\theta'_v)_o$ is the surface sensible heat flux; γ_{θ_v} is the lapse rate of potential temperature; β_{θ_v} is the ratio entrainment heat flux to surface heat flux; $\langle q\rangle_o$ is the initial slab specific humidity; Δq_o is the initial jump specific humidity; $(w'q')_o$ is the surface latent heat flux; γ_q is the lapse rate of specific humidity.

Copyright © 2007 Royal Meteorological Society

DOI: 10.1002/qj

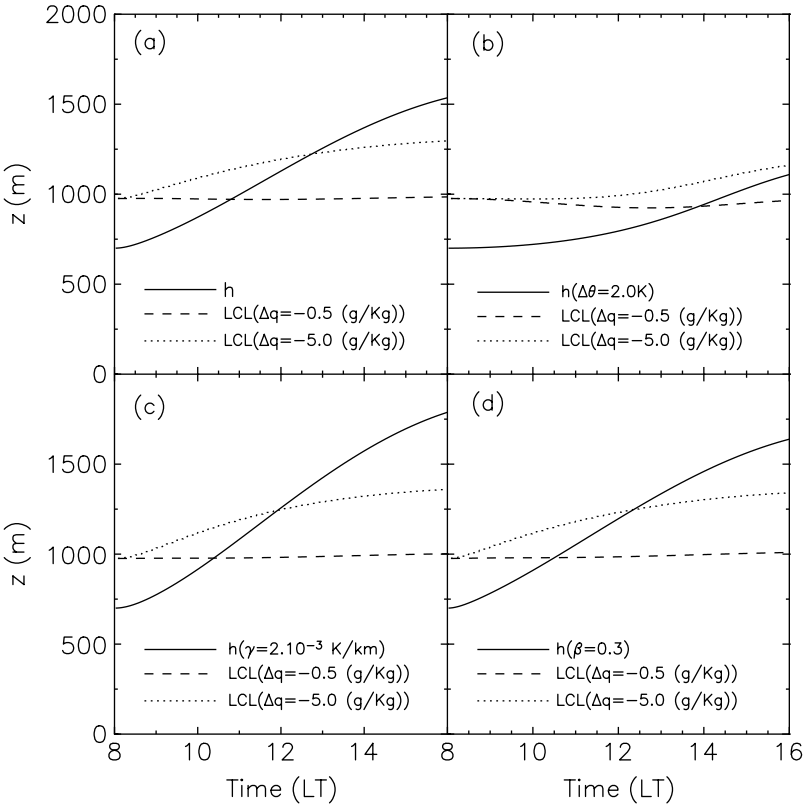

Figure 12. Time evolution of boundary-layer height h (solid lines) and LCL, for the following initial values of the moisture jump: -0.5 g/kg (dashed lines); -5.0 g/kg (dotted lines). (a) Initial values similar to the early-morning conditions at 08 LT on 21 June (see Table II). (b) As (a), but with initial $\Delta\theta = 2$ K. (c) As (a), but with $\gamma_\theta = 2 \times 10^{-3}$ K/m. (d) As (a), but with $\beta_{\theta_v} = 0.3$.

Figure 12(b) shows the same situation except that we have increased the initial jump of the virtual potential temperature at the interface to 2.0 K. This test is illustrative of the situation of the previous day (20 June), characterized by large inversion jumps for $\Delta\theta_o$ and Δq_o at the entrainment zone. A shallow boundary layer with a slow growth rate is the main feature of this sensitivity test, leading to a late onset of the condition $h = LCL$ (for the case $\Delta q_o = -0.5$ g/kg), or a cloudless boundary layer because $LCL > h$ (initial $\Delta q_o = -5.0$ g/kg).

We study the increase in atmospheric instability above the boundary layer by reducing the temperature lapse rate to 2×10^{-3} K/m (see Figure 12(c)). The boundary layer deepens faster, and the condition $h = LCL$ is attained earlier, than in the case presented in Figure 12(a). This rapid growth leads to an increase in the entrainment of dry air, yielding a higher LCL (see the case $\Delta q_o = -5.0$ g/kg). This decrease in the temperature lapse rate was also used by Brown *et al.* (2002) to reproduce, by means of the LES, shallow cumulus with an enhanced vertical development.

Finally, we show in Figure 12(d) a sensitivity test for the ratio of the entrainment heat flux to the surface heat flux. As studied by Pino *et al.* (2003) for the previous day, larger values of this ratio are expected because of the enhancement of the entrainment flux by the presence of shear at the surface and at the entrainment zone. The model results show that, in spite of the increase of warm and dry air brought into the boundary layer by the entrainment process, the condition $h = LCL$ is reached slightly earlier than in the observed case (for the case $\Delta q_o = -0.5$ g/kg), because of the more rapid growth of the boundary layer.

Although this study is conceptual, the analysis indicates the subtlety of setting up optimal conditions for the formation of shallow cumulus over land. Briefly, a decrease in the morning initial potential-temperature jump and temperature lapse rate leads to a higher rate of boundary-layer growth, increasing the probability of cloud formation. In turn, this higher rate is normally associated with larger entrainment events of warmer and drier air into the boundary layer, which can delay attainment of the condition $h = LCL$. A small jump of moisture in the entrainment region could compensate for this drying effect of the boundary layer and facilitate cloud formation.

5. Conclusions

We have investigated the role of the NBL and its layer aloft in setting up appropriate conditions for the formation of shallow cumuli. Surface and upper-air observations of two consecutive nights have been studied and compared in order to determine the processes involved in producing two different diurnal boundary layers (one clear and the other cloudy) under similar driving diurnal surface conditions. The two nights display very similar turbulent

Copyright © 2007 Royal Meteorological Society

DOI: 10.1002/qj

structure and evolution, characterized by intense turbulent mixing (friction velocities of 0.5–0.6 ms^{-1}) driven by the wind shear generated by the LLJ. However, during the second night, the air mass above the NBL is modified by a low-level advection event, becoming colder (by approximately 4 K), with a higher specific humidity content (an increase of approximately 10 g/kg). As a result, the conditions at the interface between the NBL and the layer aloft are greatly modified during the second night. We can summarize these key observed conditions favourable for cloud formation during the day as follows:

1. a reduction in the potential-temperature and moisture jump at the interface near sunrise;
2. an increase in the instability above the boundary layer during the morning transition; and
3. the possibility of rapid formation of well-mixed profiles of potential temperature and specific humidity due to high levels of turbulence at night and in the morning transition.

Using a mixed-layer model, we have demonstrated the sensitivity of the evolution of a diurnal boundary layer to changes in the initial values of the inversion potential-temperature and moisture jumps (condition 1), and to the temperature lapse rate (condition 2). Our analysis aims to determine the conditions under which the boundary-layer height exceeds the LCL. Higher boundary-layer values are found when the potential-temperature jump and the temperature lapse rate in the free troposphere are reduced. However, this enhancement is closely associated with a warmer and drier boundary layer, which leads to a higher LCL. The drying effect can be compensated for if the moisture levels in the free troposphere are fairly similar to those of the boundary layer (with a relatively small jump in moisture content in the entrainment region).

At a similar order of magnitude and range of variability of the surface turbulent conditions during the night, these three factors will lead to vertical profiles of the potential temperature and specific humidity that are optimal for triggering shallow-cumulus development over land. Thus, this study indicates the importance of accurately modelling vertical thermodynamic variables at night in order to be able to reproduce cloud formation and its thermodynamic characteristics during diurnal conditions. The high spatial density and high frequency of the vertical-profile measurements of the wind speed and direction, potential temperature and specific moisture, and of the measurements of the surface conditions around the ARM site, make this observational data set very appropriate for studying how boundary-layer processes interact with large-scale horizontal advection in mesoscale models.

Acknowledgements

The data used in this paper were obtained from the Atmospheric Radiation Measurement (ARM) Program sponsored by the US Department of Energy. ECMWF provided the ERA-40 reanalysis data. A discussion with Peter Duynkerke in summer 2001 triggered this investigation. Discussions with Louise Nuijens about the transition from clear to cloudy boundary layers were highly enlightening. The critical comments given by Roel Neggers were very useful in improving the paper, in particular with regard to the description of the large-scale forcing.

Appendix A: The mixed-layer model

The mixed-layer model equations governing the slab properties of the diurnal boundary layer are expressed in terms of:

- the temporal evolution of the boundary-layer growth, the slab of virtual potential temperature and the specific humidity; and
- the interface jump for both quantities between the free tropospheric and slab-averaged values.

The equations are derived from a vertical integration of the one-dimensional equation for heat and water vapour. For instance, the equation for the slab potential temperature is:

$$\frac{\partial \theta_{\mathrm{m}}}{\partial t} = \frac{(\overline{w'\theta'})_{\mathrm{o}} - (\overline{w'\theta'})_{\mathrm{e}}}{h}, \tag{A.1}$$

where θ_{m} is the slab potential temperature, $\overline{w'\theta'}_{\mathrm{o}}$ is the surface heat flux, $\overline{w'\theta'}_{\mathrm{e}}$ is the entrainment heat flux, and h is the boundary-layer height. The evolution of the potential-temperature jump at the interface obeys:

$$\frac{\partial \Delta\theta_{\mathrm{h}}}{\partial t} = \frac{\partial \theta_{\mathrm{h+}}}{\partial t} - \frac{\partial \theta_{\mathrm{m}}}{\partial t} = \gamma_{\theta}\left(\frac{\partial h}{\partial t} - w_{\mathrm{s}}\right) - \frac{\partial \theta_{\mathrm{m}}}{\partial t}, \tag{A.2}$$

where $\Delta\theta_{\mathrm{h}}$ is the potential-temperature jump, $\theta_{\mathrm{h+}}$ is the temperature above the mixed layer, γ_{θ} is the temperature lapse rate, and w_{s} is the mean vertical subsidence velocity. The entrainment flux is formally related to the jump at the interface through the zero-order model:

$$(\overline{w'\theta'})_{\mathrm{e}} = -w_{\mathrm{e}}\Delta\theta_{z_i} = \left(\frac{\partial h}{\partial t} - w_{\mathrm{s}}\right)\Delta\theta_{z_i}, \tag{A.3}$$

where w_{e} is the entrainment velocity.

Similar equations hold for the specific humidity q. In our study, we prescribe the surface fluxes, the temperature and specific-moisture lapse rates, and the subsidence velocity. In addition, we prescribe the initial conditions for the virtual potential temperature and specific humidity (see Table II). Therefore we only need to apply a closure for the relation between the surface heat flux and the entrainment heat flux: we use the value $\beta_{\theta_{\mathrm{v}}} = 0.2$.

References

Berg LK, Stull RB. 2006. 'Evaluation of a new parametertization for fair-weather cumulus'. Paper number J7.6 in *Proceedings of the 17th*

Copyright © 2007 Royal Meteorological Society

DOI: 10.1002/qj

Symposium on Boundary Layers and Turbulence, June 22–25, San Diego (USA).

Brown AR, Cederwall RT, Chlond A, Duynkerke PG, Golaz JC, Khairoutdinov JM, Lewellen DC, Lock AP, Macveen MK, Moeng CH, Neggers RAJ, Siebesma AP, Stevens B. 2002. Large-eddy simulation of the diurnal cycle of shallow cumulus convection over land. *Q. J. R. Meteorol. Soc.* **128**: 1075–1094.

Cheinet S, Beljaars A, Köhler M, Morcette JJ, Viterbo P. 2005. Assesing physical processes in the ECMWF model forecast using the ARM SGP observations. *ECMWF–ARM Report Series* **1**: 1–25.

Conangla L, Cuxart J. 2006. On the turbulence in the upper part of the low-level jet: an experimental and numerical study. *Boundary-Layer Meteorol.* **118**: 379–400.

Dudhia J. 1993. A non-hydrostatic version of the Penn State-NCAR mesoscale model: validation tests and simulation of an Atlantic cyclone and cold front. *Mon. Wea. Rev.* **121**: 1493–1513.

Ek MB, Holtslag AAM. 2004. Influence of soil moisture on boundary-layer cloud development. *J. Hydrometeorol.* **5**: 86–99.

Higgins RW, Yao Y, Yaroshi ES, Janowiak JE, Mo KC. 1997. Influence of the Great Plains Low-Level Jet on sumertime precipitation and moisture transport over Central United States. *J. Climate* **10**: 481–507.

Lenderink G, Siebesma AP, Cheinet S, Irons S, Jones CG, Marquet P, Müller F, Olmeda D, Calvo J, Sanchez E, Soares PMM. 2004. The diurnal cycle of shallow cumulus clouds over land: a single column model intercomparison study. *Q. J. R. Meteorol. Soc.* **130**: 3339–3364.

Lilly DK. 1968. Models of cloud-topped mixed layers under a strong inversion. *Q. J. R. Meteorol. Soc.* **94**: 292–309.

Nakamura R, Mahrt L. 2006. Vertically integrated sensible-heat budgets for stable nocturnal boundary layers. *Q. J. R. Meteorol. Soc.* **123**: 383–403.

Neggers RAJ, Siebesma AP, Lenderink G. 2004. An evaluation of mass flux closures for diurnal cycles of shallow cumulus. *Mon. Weather Rev.* **132**: 2525–2538.

Pino D, Vilà-Guerau de Arellano J, Duynkerke PG. 2003. The contribution of shear to the evolution of a convective boundary layer. *J. Atmos. Sci.* **60**: 1913–1926.

Tennekes H. 1973. A model for the dynamics of the inversion above a convective boundary layer. *J. Atmos. Sci.* **30**: 558–567.

Uppala SM, Kållberg PW, Simmons AJ, Andrae U, da Costa Bechtold V, Fiorino M, Gibson JK, Haseler J, Hernandez A, Kelly GA, Li X, Onogi K, Saarinen S, Sokka N, Allan RP, Andersson E, Arpe K, Balmaseda MA, Beljaars ACM, van de Berg L, Bidlot J, Bormann N, Caires S, Chevallier F, Dethof A, Dragosavac M, Fisher M, Fuentes M, Hagemann S, Hólm E, Hoskins BJ, Isaksen L, Janssen PAEM, Jenne R, McNally AP, Mahfouf J-F, Morcrette J-J, Rayner NA, Saunders RW, Simon P, Sterl A, Trenberth KE, Untch A, Vasiljevic D, Viterbo P, Woollen J. 2005. The ERA-40 re-analysis. *Q. J. R. Meteorol. Soc.* **131**: 2961–3012. DOI: 10.1256/qj.04.176

Zhu P, Albrecht B. 2002. A theoretical and observational analysis on the formation of fair-weather cumuli. *J. Atmos. Sci.* **59**: 1983–2005.

Zhu P, Albrecht B. 2003. Large eddy simulations of continental shallow cumulus. *J. Geophys. Res.* **108**: 51–57.

Copyright © 2007 Royal Meteorological Society